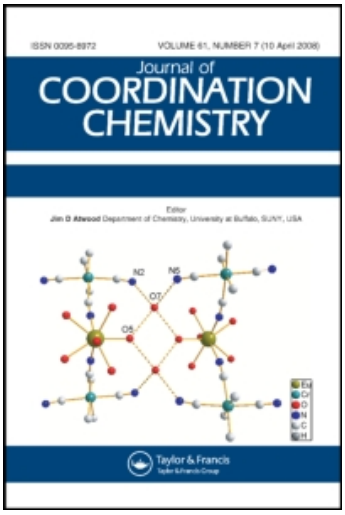

Journal of Coordination Chemistry
Publication details, including instructions for authors and subscription information:
http://www.informaworld.com/smpp/title~content=t713455674

Iron complexes of new hydrophobic derivatives of *tris*(2-pyridylmethyl)amine: synthesis, characterization, and catalysis of alkane oxygenation by H_2O_2

Gregorio Guisado-Barrios[a]; Alexandra M. Z. Slawin[a]; David T. Richens[a]
[a] EaStCHEM School of Chemistry, University of St. Andrews, Fife KY16 9ST, Scotland, UK

First published on: 06 August 2010

To cite this Article Guisado-Barrios, Gregorio , Slawin, Alexandra M. Z. and Richens, David T.(2010) 'Iron complexes of new hydrophobic derivatives of *tris*(2-pyridylmethyl)amine: synthesis, characterization, and catalysis of alkane oxygenation by H_2O_2', Journal of Coordination Chemistry, 63: 14, 2642 — 2658, First published on: 06 August 2010 (iFirst)
To link to this Article: DOI: 10.1080/00958972.2010.506216
URL: http://dx.doi.org/10.1080/00958972.2010.506216

Journal of Coordination Chemistry
Vol. 63, Nos. 14–16, 20 July–20 August 2010, 2642–2658

Iron complexes of new hydrophobic derivatives of *tris*(2-pyridylmethyl)amine: synthesis, characterization, and catalysis of alkane oxygenation by H_2O_2

GREGORIO GUISADO-BARRIOS,
ALEXANDRA M.Z. SLAWIN and DAVID T. RICHENS*

EaStCHEM School of Chemistry, University of St. Andrews,
North Haugh, St. Andrews, Fife KY16 9ST, Scotland, UK

(*Received 16 February 2010; in final form 20 May 2010*)

Several new iron(II) triflate complexes of 6-py-substituted derivatives of *tris*(2-pyridylmethyl) amine (TPA); $[Fe(\mathbf{3–6})(CH_3CN)_x](CF_3SO_3)_2$ (**3** = *tris*-(6-methoxymethyl-2-pyridylmethyl) amine, $x = 0$; **4** = *tris*-(6-octoxymethyl-2-pyridylmethyl)amine, $x = 0$; **5** = 6-(*N*′-hexylureido-2-pyridylmethyl)-*bis*(2-pyridylmethyl)amine, $x = 1$; and **6** = *bis*-(6-(*N*′-hexylureido)-2-pyridylmethyl)-2-pyridylmethylamine) have been synthesized to probe the introduction of a hydrophobic peralkyl chain (**4–6**) and hydrogen-bonding (from urea N–H) (**4** and **5**) on the selective catalysis of alkane oxygenation by H_2O_2 in CH_3CN. For $[Fe(\mathbf{6})](CF_3SO_3)_2$, hexadentate coordination of iron involving the two urea carbonyls was confirmed by X-ray structural analysis. Despite this, $[Fe(\mathbf{6})](CF_3SO_3)_2$ exhibited the highest A/K ratio (3.3), yet seen for catalysis of H_2O_2 oxygenation of cyclohexane by an iron(II) complex of a *bis*(6-py)- or *tris*(6-py)-substituted TPA derivative. This has been tentatively attributed to a degree of O–O cleavage assistance within high spin seven-coordinate $[Fe(\mathbf{6})OOH]^{2+}$ *via* urea N–H protonation of the departing ''OH'' leading to participation from oxo-iron(IV) or (V) intermediates. The lack of similar hydrogen-bonding assistance results in $[Fe(\mathbf{6})OOBu^t]^{2+}$ being one of the most long-lived high spin peroxoiron(III) complexes yet synthesized ($t_{1/2} = 1.3$ h at 298 K).

Keywords: Iron; Tris-(2-pyridylmethyl)amine; Alkane oxidation; Catalysis

1. Introduction

Extensive catalysis and spectroscopic studies by Que [1–7], Britovsek *et al*. [8], Rybak-Akimova [9], Comba [10], and Talsi [11] have shown that *bis*(acetonitrile)(*tris*(2-pyridylmethyl)amine)iron(II), $[Fe(TPA)(CH_3CN)_2]^{2+}$ **1** and related species are efficient catalysts of alkene epoxidation/*cis*-dihydroxylation and cycloalkane hydroxylation by hydrogen peroxide and other peroxy reagents in CH_3CN. Several iron–TPA complexes including **1** have been patented as catalysts for alkaline bleaching [12]. The oxygenating activity of **1** is believed to stem from the formation of reactive high-valent oxo–iron intermediates and the tetradentate nature of TPA which leads to the reactive oxo group located *cis* to a labile coordination site [1, 2, 5, 7, 13]. It appears that two basic

*Corresponding author. Email: dtr@st-andrews.ac.uk

Journal of Coordination Chemistry
ISSN 0095-8972 print/ISSN 1029-0389 online
DOI: 10.1080/00958972.2010.506216

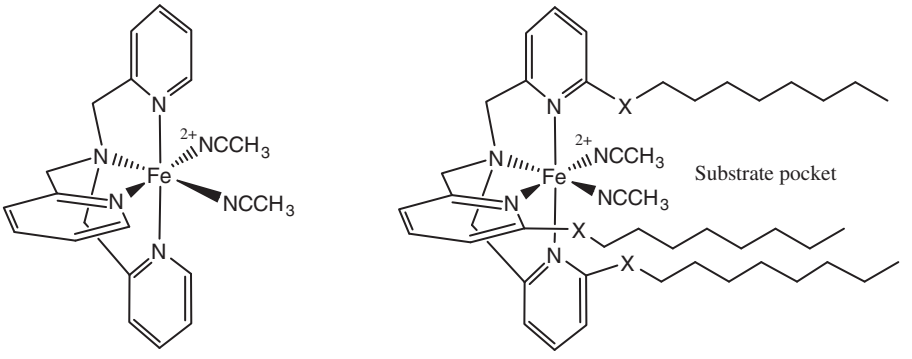

1 **2**

Figure 1. Structure of **1** and of its tris-6-py-peralkylated version.

pathways to ROOH activation starting from iron(II) may be involved in generating the reactive oxygenating center consistent with the experimental observations and, in particular, promotion of the activity in the presence of carboxylic acids [14]: (1) an activated hydroperoxide (AH) pathway and (2) a percarboxylic acid (PC) pathway. It is believed that alkene epoxidation and cycloalkane hydroxylation are predominantly carried out by a short-lived highly reactive oxo–iron(V) species [14], whereas alkene *cis*-dihydroxylation and, to a lesser extent epoxidation, are attributable to iron(IV) [10]. While the alkene epoxidation/*cis*-dihydroxylation activity shown by **1** covers a range of alkene skeletons and even arenes [9, 15], the corresponding activity toward C–H oxygenation/hydroxylation is restricted to cycloalkanes, activated arenes, and substrates with reactive benzylic CH_2 groups, e.g., ethylbenzene. The reactivity toward linear alkanes is especially poor and nonselective and, where observed, favors the more reactive internal methylenes [16]. A much sought after process industrially is the selective 1-hydroxylation of linear alkanes, especially those from the C_7–C_{12} petroleum fraction, to alcohol and aldehyde oxygenates [17] which are important precursors to a range of surfactants and detergent additives and as plasticizers for PVC. One way of achieving terminal C–H reaction on a linear alkane would be to use substrate orientation control within which only the terminal C–H bonds are close to the oxygenating center. One method of achieving this would be to construct a hydrophobic channel/pocket built onto the catalyst. Such hydrophobic channels/pockets are believed central to the regioselectivity shown by several P450-dependent alkane monooxygenases [18–20]. Figure 1 shows how TPA upon metal complexation directs the 6-substituent positions on the three pyridine rings to orientate themselves along the same direction. Subsequent 6-py-peralkylation, **2** would then quickly assemble a threefold symmetrical hydrophobic pocket encapsulating the reactive iron–oxo center generated *via* reaction with ROOH reagents at the two replaceable *cis* sites on the iron.

Herein, we report the synthesis and characterization of iron(II)/(III) complexes of four new 6-py-alkylated TPA ligands **3–6** along with *tris*(6-bromo-2-pyridylmethyl) amine **7** (figure 2). The products of the reaction of the iron(II) complexes of **3–6** with ROOH (R=H or t-Bu) reagents have been investigated by electron paramagnetic resonance (EPR) and UV-Vis spectroscopy along with a preliminary investigation of

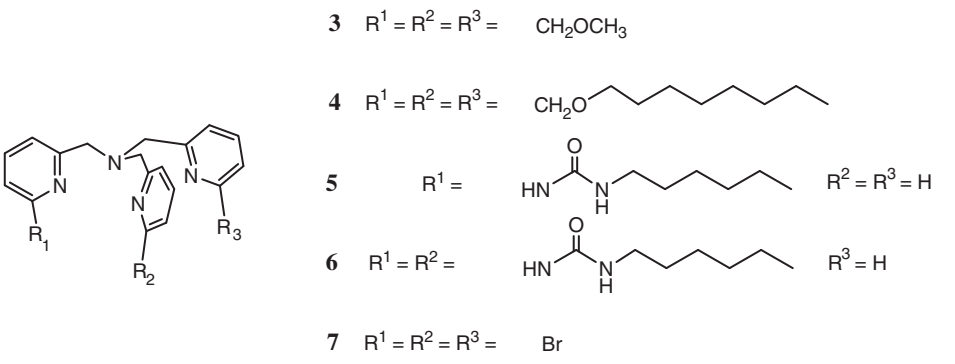

Figure 2. Ligands **3**–**7** synthesized and studied in this work.

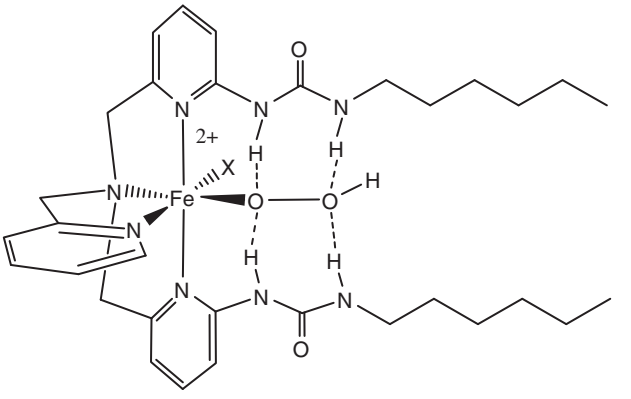

Figure 3. A putative hydroperoxoiron(III) complex of **6** showing how urea–OOH hydrogen-bonding could self-assemble the hydrophobic channel.

catalytic activity toward the hydrogen peroxide oxygenation of cyclohexane in CH_3CN. Use of the urea spacer group in **5** and **6** arose from the idea that the urea N–H groups might form a hydrogen-bond to the OOH^- ligand on the iron(III) precursor complex promoting the self-assembly of the hydrophobic channel (figure 3), while facilitating heterolytic O–O cleavage (*via* hydrogen-bond assisted loss of OH^-) to generate a potent oxo–iron(V) oxidant. Cyclohexane was chosen as the initial substrate since the alcohol/ketone (*A*/*K*) ratio can be used as a reliable probe for the involvement of non-radical high-valent oxo–iron intermediates [1–7, 8, 21].

2. Experimental

2.1. *Materials and chemicals*

All chemicals and reagents purchased, including 2-aminomethylpyridine and *bis*(2-picolyl)amine, were used as received. DMF and CH_3CN were both dried over

calcium hydride overnight followed by distillation. $[Fe(O_3SCF_3)_2(CH_3CN)_2]$ was prepared as an air sensitive off-white solid by reacting iron metal and anhydrous CF_3SO_3H in CH_3CN followed by crystallization with diethyl ether [22]. The solid was stored under nitrogen prior to use. Full details of the synthesis and characterization of ligands **3**–**7** and of their iron(II) complexes are given in the "Supplementary material."

2.2. *Physical measurements*

X-ray crystallography was carried out at 93(2) K using Mo-Kα radiation from a Rigaku MM007 rotating anode diffractometer operating with a low-temperature attachment. ^{1}H- and ^{13}C-NMR spectra were recorded on a Bruker Avance 300 and 400 spectrometers (300 or 400.13 MHz for ^{1}H, 75.4 MHz for ^{13}C, and 282 MHz for ^{19}F). Electrospray mass spectra were acquired on a Water's 2795 HPLC with Micromass LCT equipped with a lock spray for accurate mass measurements. C, H, and N analyses were carried out on dried samples using a Carlo Erba CHNS analyzer. Time-dependent UV-Vis–NIR spectra were recorded in acetonitrile solution at 25°C on a Perkin Elmer Lambda 14 scanning double-beam spectrophotometer in 1 cm quartz cuvettes. EPR spectra were recorded at 110 K in $12 \times 0.4\,cm^2$ i.d. quartz tubes on a Bruker EMX 10/12 spectrometer operating at 9.5 GHz with 100 kHz modulation.

2.2.1. Catalysis of cyclohexane oxygenation with H_2O_2. The oxygenation reactions were carried out in acetonitrile at 25°C under air. Each iron(II) complex was assembled in acetonitrile solution *in situ via* addition of one equivalent of ligand to one equivalent of $[Fe(CH_3CN)_2(O_3SCF_3)_2]$ and then diluted as required. Aqueous solutions of 30% w/w hydrogen peroxide were standardized by titration with potassium permanganate. The reactions were initiated by the addition of a diluted hydrogen peroxide solution in acetonitrile (70 mmol L^{-1}, 10 equivalents or 700 mmol L^{-1}, 100 equivalents) to an acetonitrile solution of the iron(II) complex (2.1 μmol, 1 equivalent) and cyclohexane (2.1 mmol, 1000 equivalents) by means of a syringe pump over a 30 min period at 25°C. Use of the syringe pump, ensured that decomposition of H_2O_2 was minimized. The large excess of substrate employed minimized overoxidation of cyclohexanol (A) to cyclohexanone (K). After syringe pump addition, the solution was stirred for another 5 min before work up. The iron(II) catalyst was removed by passing the solution through silica gel followed by elution with 3 cm^3 of CH_3CN [3]. An internal standard (toluene) was added at this point, and the solution was subjected to GC analysis. This was carried out on an Agilent 6890A chromatograph with HP-5 column (30 m × 0.25 mm, film thickness 0.25 μm). The products were identified by GC–MS comparison with authentic compounds. All reactions were run at least in duplicate, and the data reported are the average of two runs. The yields reported are based on the amount of oxidant (H_2O_2) converted into oxygenated products. Two series of catalytic experiments were carried out using both 10 and 100 equivalents of H_2O_2 following the methodology previously reported by Que and co-workers [2–4] and Britovsek *et al.* [8].

3. Results and discussion

3.1. *Characterization of iron complexes*

Each of the iron(II) complexes was prepared *in situ* by addition of an equimolar quantity of **3**–**7** in CD_3CN under a nitrogen atmosphere to a pale yellow deoxygenated solution of $[Fe(CH_3CN)_2(O_3SCF_3)_2]$ in CD_3CN yielding a reddish orange solution exhibiting ^{1}H-NMR resonances in the range from 0 to +100 ppm (figures S1, S2, S5–S8), consistent with the presence of high spin iron(II) complexes. For $[Fe(\mathbf{3})]^{2+}$, the strong downfield positions of the methylene and methoxy groups at 41 and 31 ppm, respectively, contrasts with the −28 ppm resonance for the methyl group in high spin $[Fe(6\text{-}Me_3TPA)(CH_3CN)_2]^{2+}$ [23] suggesting that all three ether oxygens strongly interact with iron(II). For this, there are two possibilities: (1) a six-coordinate structure in rapid fluxional equilibrium on the NMR timescale with a seven-coordinate species [24] having all three pendent ether groups attached (figure 4a); or (2) the seven-coordinate species alone (figure 4b). The strong peak in the solution ES^+ MS spectrum (CH_3CN solution) at m/z 627 is assignable to $[Fe(\mathbf{3})(O_3SCF_3)]^+$. Solutions of $[Fe(\mathbf{3})]^{2+}$ in CD_2Cl_2 show a strong sharp ^{19}F-NMR resonance at −78 ppm consistent with the presence of free $CF_3SO_3^-$ [25] (figure S3). A similar, but much broader ^{19}F-NMR resonance is seen at −70 ppm from a solution of $[Fe(\mathbf{3})]^{2+}$ prepared in CD_3CN (figure S4). The origin of this broadening is not clear, but may be a further reflection of the fluxional nature of the coordination sphere at the iron center of $[Fe(\mathbf{3})]^{2+}$ in CD_3CN solution (figure 4).

Similar evidence for coordination of all three ether oxygens is apparent in $[Fe(\mathbf{4})]^{2+}$ by the ^{1}H-NMR resonances for the two methylene groups on either side of the ether oxygen appearing noticeably downfield at 34 and 36 ppm, respectively (figure S5). The strong peak in the solution ES^+ MS spectrum (CH_3CN solution) at m/z 921 is assignable to the cation $[Fe(\mathbf{4})(O_3SCF_3)]^+$.

In the case of $[Fe(\mathbf{5})]^{2+}$, the downfield resonance of the first methylene of the *n*-hexyl chain (18.4 ppm) (figure S7), implies again a significant interaction with the paramagnetic iron(II) center. Coordination of the urea carbonyl was subsequently suggested by a strong peak in the ES^+ MS spectrum at m/z 487 for the ion $[Fe(\mathbf{5})\text{–}H]^+$ (deprotonated urea group) but no peak at m/z 637 for the triflate complex $[Fe(\mathbf{5})(O_3SCF_3)]^+$. The deprotonated urea is presumed to occupy the triflate site. Similar findings were

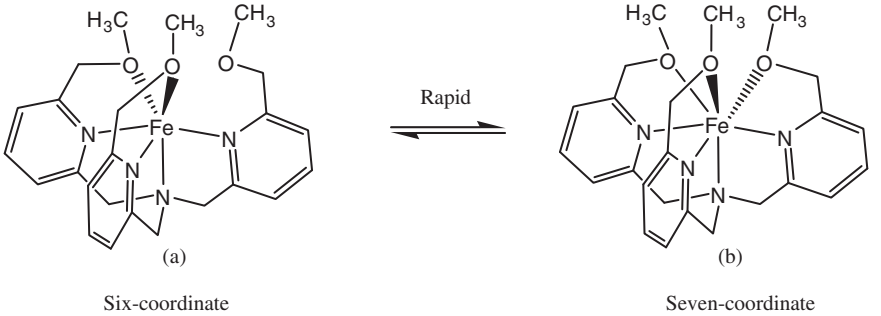

Figure 4. Proposed fluxional equilibrium between six-coordinate and seven-coordinate **3** in high spin $[Fe(\mathbf{3})](CF_3SO_3)_2$ in CH_3CN.

apparent in the ES^+ MS of [Fe(**6**)]$(O_2SCF_3)_2$ wherein urea carbonyl coordination has been directly confirmed by X-ray crystallography.

Crystals of [Fe(**6**)]$(O_2SCF_3)_2$ grown from CH_3CN solution following vapor diffusion of diethyl ether were found to be suitable for X-ray analysis. Figure 5 shows the molecular structure. The iron(II) center is six-coordinate to four nitrogens of TPA plus two carbonyl oxygens from the 6-*N*-hexylureido substituents. Bond lengths and angles are given in table S3. The Fe–N bond lengths are in the typical range for high spin iron(II) complexes of TPA-type ligands. Coordination of amide carbonyl oxygen is not unusual for iron(II) and indeed the structure of $[Fe(\mathbf{6})]^{2+}$ is very similar to that of the iron(II) complex $[Fe(BPPA)]^{2+}$ reported by Masuda *et al.* [26] wherein the iron is similarly coordinated to four TPA nitrogens and two carbonyls from 6-pivaloylamido substituents. The octahedral geometry is highly distorted away from regular octahedral with distinctly different Fe–O bond lengths, 2.018(4) and 2.185(4) to the two urea carbonyls. There was no evidence of the uniquely long Fe–N bond to the tertiary amine nitrogen that characterizes seven-coordinate iron(III)–TPA centers such as those present in $[Fe_3L_2](ClO_4)_3$ (H_3L = *tris*(6-hydroxymethyl-2-pyridylmethyl)amine) [27]. Indeed, the longest Fe–N bond is to one of the pyridines carrying a 6-*N*′-hexylureido substituent. Finally, each of the urea N–H groups is hydrogen-bonded to two triflate counter anions. The downfield shifted resonance for the first CH_2 group of the *n*-hexyl chain, 32 ppm (figure S8 and table S2) suggests retention of the urea carbonyl coordination in CH_3CN solution. This was also implied by the presence of a strong peak at m/z 629 in the ES^+ MS for $[Fe(\mathbf{6})-H]^+$ (deprotonation of one urea group) but no peak for $[Fe(\mathbf{6})(O_3SCF_3)]^+$.

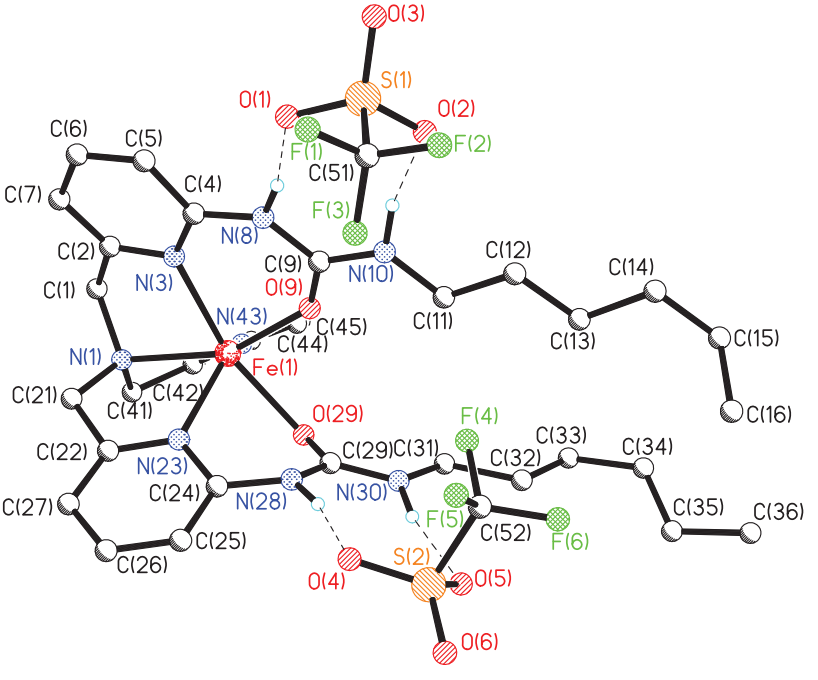

Figure 5. Molecular structure of [Fe(**6**)]$(O_2SCF_3)_2$.

The presence of two hydrogen-bonded urea groups to triflate anions in $[Fe(\mathbf{6})]^{2+}$ is presumed responsible for the favorable crystal packing leading to lower solubility and crystallization. Finally, as a result of urea carbonyl coordination, both of the *n*-hexyl groups are oriented on one side of the complex forming an apparent hydrophobic channel (tail) adjacent to the iron coordination center. This was one of the features hoped for in this family of hydrophobic peralkyl-substituted Fe–TPA complexes.

Despite the evidence of urea carbonyl coordination in $[Fe(\mathbf{6})]^{2+}$ and $[Fe(\mathbf{5})(CH_3CN)]^{2+}$, it was nonetheless hoped that subsequent reaction with H_2O_2 to form a hydroperoxoiron(III) complex (explored below) would result in urea carbonyl oxygen dissociation to facilitate the intended hydrogen-bonded interaction of urea N–H with the hydroperoxo group (figure 3), rather than retention of amide oxygen coordination as seen in $[Fe(BPPA)(O_2CBu^t)]^{2+}$ [26].

3.2. *Reaction of H_2O_2 and t-BuOOH with $[Fe(3)]^{2+}$ and $[Fe(4)]^{2+}$*

Figure 6 shows the EPR spectra at 110 K obtained after mixing and rapid freezing of a solution of $[Fe(\mathbf{3})]^{2+}$ with; (a) H_2O_2 and (b) t-BuOOH. Reaction with H_2O_2 gives a strong signal at $g = 4.4$ flanked by weaker features either side consistent with a high spin iron(III) center in full rhombic symmetry ($E/D = 1/3$). Similar features indicative of a

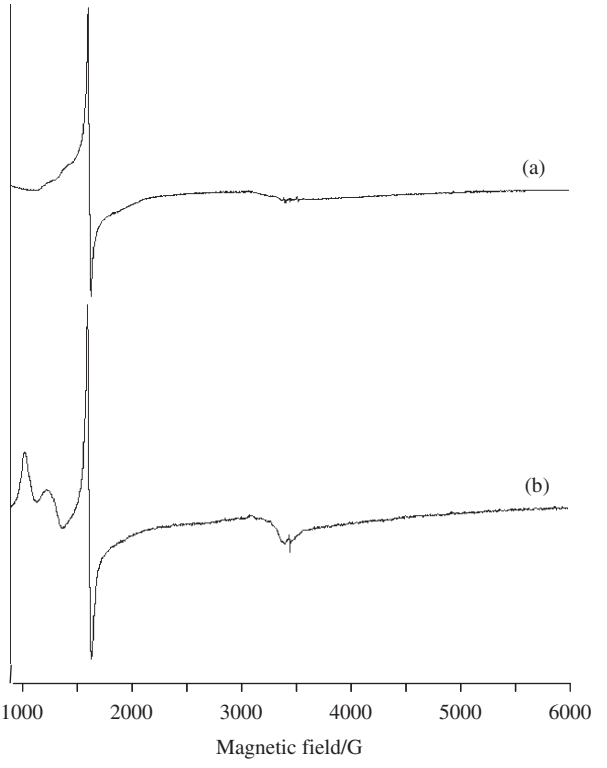

Figure 6. Frozen-glass X-band EPR spectra (110 K, CH_3CN) following mixing of $[Fe(\mathbf{3})]^{2+}$ with (a) H_2O_2 and (b) t-BuOOH.

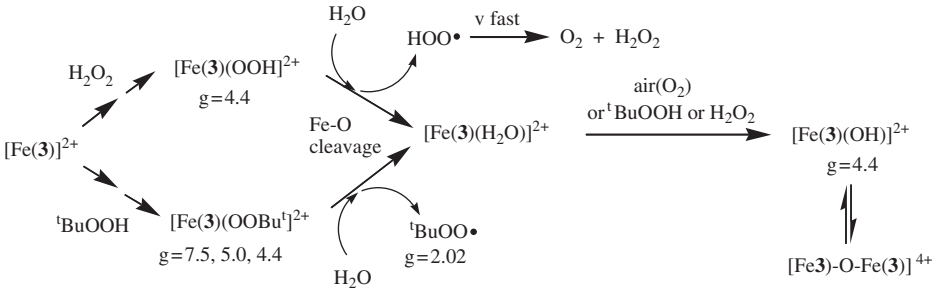

Figure 7. Proposed reaction pathways involving reaction of $[Fe(\mathbf{3})]^{2+}$ (shown) and $[Fe(\mathbf{4})]^{2+}$ with H_2O_2 and t-BuOOH in CH_3CN solvent.

high spin iron(III) center in intermediate symmetry are apparent from the corresponding reaction with t-BuOOH: intense signal at $g = 4.4$ accompanied by weaker features at $g = 7.5$, 5.0, and 2.0. Both sets of features correlate with the appearance of an intense purple color assignable to peroxoiron(III) complexes [2] which fades in intensity upon partial warming and re-freezing. In the case of (b), the warming is accompanied by the appearance and then slow decay of a strong sharp signal at $g = 2.02$ for the *t*-butylperoxyl radical (figure S9) [28]. Eventually, the EPR features of $[Fe(\mathbf{3})OOBu\text{-}t]^{2+}$ fade completely following warming over several hours to be replaced by a weaker low-field feature with $g = 4.4$ (figure S9), assignable to the high spin complex $[Fe(\mathbf{3})(OH)]^{2+}$. The solution color at this point was deep yellow–brown. A scheme of likely reactions taking place is illustrated in figure 7. The EPR spectra of $[Fe(\mathbf{3})(OOH)]^{2+}$ and $[Fe(\mathbf{3})OOBu\text{-}t]^{2+}$ are reminiscent of the features observed for $[Fe(BPPA)(O_2CBu^t)]^{2+}$ [26] suggesting a similar seven-coordinate high spin iron(III) center. Hepta coordination around iron is also apparent in other high spin d^5 complexes of TPA ligands with pendent CH_2OR groups substituted at the 6-py positions as exemplified by $[Fe_3L_2](ClO_4)_3$ and $[Mn(H_3L)]Cl_2$ (H_3L = *tris*(6-hydroxymethyl-2-pyridylmethyl)amine) [27]. Similar behavior was apparent in the reactions of $[Fe(\mathbf{4})]^{2+}$ with both H_2O_2 and t-BuOOH indicating little or no effect on the iron species formed from the presence of longer *n*-octyl chain.

3.2.1. Reaction of H_2O_2 and t-BuOOH with $[Fe(\mathbf{5})(CH_3CN)]^{2+}$. Here, there was a marked difference in the behavior toward the two peroxide reactants. The reaction of $[Fe(\mathbf{5})(CH_3CN)]^{2+}$ with a 100-fold excess of H_2O_2 at 25°C was characterized by the appearance of a persistent pink color characterized by a shoulder near 500 nm (figure 8), which decayed only slowly over a period of 3 h to give a final yellow–brown solution. The decay, monitored at 530 nm, was exponential (figure 7 inset), giving a first-order rate constant at 25°C of $(6.33 \pm 0.03) \times 10^{-4}\,s^{-1}$ and a half-life of 18.2 min. The reaction of $[Fe(\mathbf{5})(CH_3CN)]^{2+}$ with H_2O_2 was also monitored by EPR in frozen solution. The addition of 100-fold excess of H_2O_2 followed by rapid freezing resulted in the appearance of a rhombic EPR signal (figure 9a), with $g_1 = 2.24$, $g_2 = 2.16$, and $g_3 = 1.94$. These signals are similar to those assigned to low spin $[Fe(TPA)(OOH)]^{2+}$ ($g_1 = 2.19$, $g_2 = 2.15$, and $g_3 = 1.97$) [4, 11]. Here, the presence of the single ureiyl substituent in **5** leads to strengthening of the overall "TPA" ligand field compared with $[Fe(\mathbf{3})]^{2+}$ and $[Fe(\mathbf{4})]^{2+}$. A number of weaker features are also seen around $g = 2.08$ and

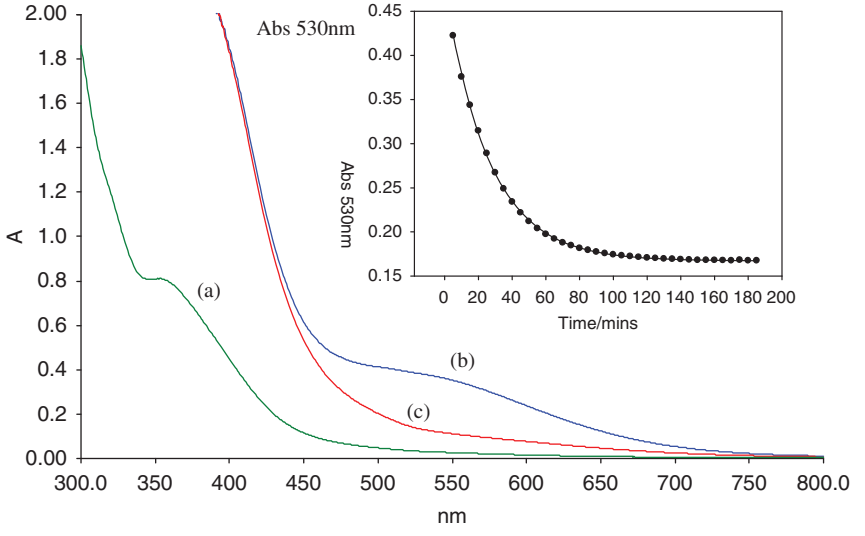

Figure 8. UV-Vis spectra for a 2.3×10^{-3} mol dm^{-3} solution of (a) [Fe(**5**)(CH$_3$CN)]$^{2+}$; (b) following addition of a 100-fold excess of aqueous H_2O_2; and (c) final spectrum after the decay of (b). (inset – exponential fit of the decay of (b) to (c) monitored at 530 nm).

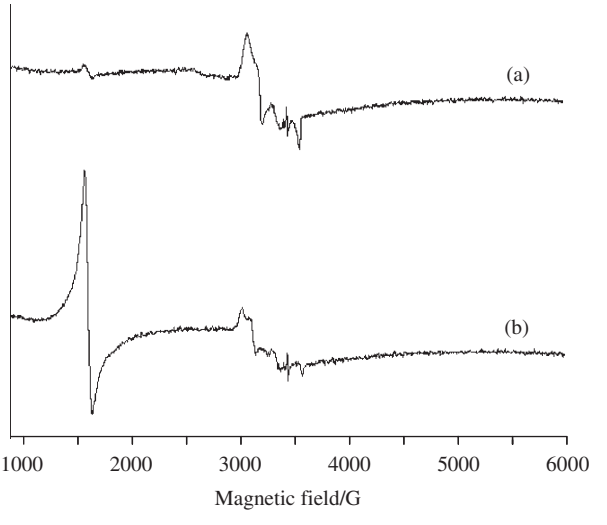

Figure 9. Frozen-glass X-band EPR spectra (110 K, CH_3CN solvent) of (a) [Fe(**5**)(CH$_3$CN)]$^{2+}$ (3×10^{-4} mol dm^{-3}) following the addition of 100-fold excess of H_2O_2 and (b) following warming to 25°C for 1 h.

$g = 2.00$. A weak high spin feature is also seen around $g = 4.4$. Warming the solution to 25°C for 1 h results in partial decay of the low spin features with concurrent increase in the high spin feature at $g = 4.4$ (figure 9b). Eventually over a period of several hours (not shown), the low spin signals are lost at the expense of the $g = 4.4$ signal. This signal is tentatively assigned to the high spin ferric complex [Fe(**5**)(OH]$^{2+}$. Also apparent throughout is a very broad underlying feature centered at $g = 2$.

The reaction of $[Fe(\mathbf{5})(CH_3CN)]^{2+}$ with a similar 100-fold excess of t-BuOOH, however, was markedly different. Mixing at low temperature (−60°C) produced a deep blue color which decayed within a few seconds at 25°C. The reaction was followed by EPR in frozen CH_3CN solution (figure 10). Immediately apparent following mixing was the appearance of a set of rhombic EPR features characteristic of a low spin iron(III) complex with $g_1 = 2.21$, $g_2 = 2.15$, and $g_3 = 1.97$ (figure 10a), which accompanies the appearance of the intense blue color. These signals are very similar to those reported for low spin $[Fe(TPA)(OOBu\text{-}t)]^{2+}$ ($g_1 = 2.19$, $g_2 = 2.15$, and $g_3 = 1.98$) and low spin $[Fe(6\text{-}MeTPA)(OOBu\text{-}t)]^{2+}$ ($g_1 = 2.20$, $g_2 = 2.12$, and $g_3 = 1.97$) [23] and are similarly assigned to low spin $[Fe(\mathbf{5})(OOBu\text{-}t)]^{2+}$, reflective again of a stronger ligand field for **5** compared to the tri-ether-substituted TPA ligands **3** and **4**. Also apparent is a sharp signal at $g = 2.02$ from the t-butylperoxyl radical. Warming for a few minutes followed by rapid re-freezing resulted in a gradual decrease in intensity of the features on either side of $g = 2$ accompanied by a steady rise in the appearance of a low-field signal at

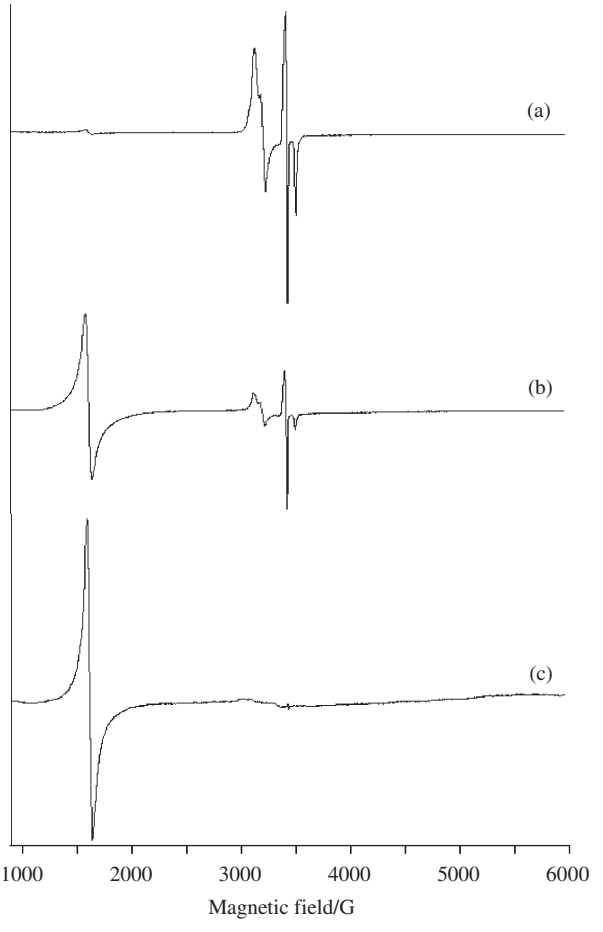

Figure 10. Frozen-glass X-band EPR spectra (110 K, CH_3CN solvent) of (a) $[Fe(\mathbf{5})(CH_3CN)]^{2+}$ following the addition of 100-fold excess of t-BuOOH; (b), (a) following warming to 25°C for 2 min; and (c), (a) following warming to 25°C for 10 min.

$g = 4.4$ (figure 10b). This signal, along with a weak broad signal at $g = 2$, eventually become the dominant features of the spectrum following warming to 25°C for 10 min (figure 10c), and as in the reaction with H_2O_2, are assigned to high spin $[Fe(\mathbf{5})(OH)]^{2+}$.

The origin of the t-BuOO$^\bullet$ radical would be initially assumed to arise from favorable Fe–O cleavage of $[Fe(\mathbf{5})(OOBu\text{-}t)]^{2+}$ as proposed in the case of $[Fe(\mathbf{3})]^{2+}$ allowing t-BuOO$^\bullet$ to persist in the low-temperature solutions [29]. However, an additional possibility for low spin peroxo complexes such as $[Fe(\mathbf{5})(OOBu\text{-}t)]^{2+}$ is homolytic O–O cleavage (1, 2) to generate an EPR silent oxo–iron(IV) intermediate along with either HO$^\bullet$ or t-BuO$^\bullet$ [1, 7, 21], the latter persisting enough at the low temperatures to abstract H from the excess t-BuOOH present to generate the longer lived t-BuOO$^\bullet$ radical which is then subsequently observed by EPR (figure 10).

$$[Fe(\mathbf{5})(OOBu\text{-}t)]^{2+} \xrightarrow{\text{homolytic O–O}} [Fe(\mathbf{5})(O)]^{2+} + \text{t-BuO}^\bullet \quad (1)$$

$$\text{t-BuO}^\bullet + \text{t-BuOOH} \longrightarrow \text{t-BuOH} + \text{t-BuOO}^\bullet \quad (2)$$

3.2.2. Reaction of H_2O_2 and t-BuOOH with $[Fe(\mathbf{6})]^{2+}$. Here, as with $[Fe(\mathbf{5})(CH_3CN)]^{2+}$, the behavior of $[Fe(\mathbf{6})]^{2+}$ toward the two oxidants is markedly different and also different to the reaction with $[Fe(\mathbf{5})(CH_3CN)]^{2+}$. The reaction of $[Fe(\mathbf{6})]^{2+}$ with a 100-fold excess of H_2O_2 at 25°C resulted in the immediate appearance of a yellow–brown color but without the appearance of the persistent pink species that had characterized the reaction with $[Fe(\mathbf{5})(CH_3CN)]^{2+}$. The EPR spectra obtained following mixing in frozen solution also failed to show evidence of a discrete intermediate species with only the gradual appearance of a low-field feature at $g = 4.4$, which correlated with the appearance of the final yellow–brown solution. The reaction with t-BuOOH, however, was completely different. Addition of a 100-fold excess of t-BuOOH to a solution of $[Fe(\mathbf{6})]^{2+}$ in CH_3CN at 25°C resulted in the appearance of a persistent intense blue color which only decayed slowly over a period of 10 h. The blue species is characterized by a peak at 603 nm ($\varepsilon = 1000\ dm^3\ mol^{-1}\ s^{-1}$) (figure 11). The decay of this species, monitored at 603 nm, was exponential (figure 11 inset), giving rise to a rate constant at 25°C of $(1.47 \pm 0.01) \times 10^{-4}\ s^{-1}$ and a half-life of 1.3 h. This reaction was also followed by EPR. Figure 12(a) shows the spectrum obtained following mixing of $[Fe(\mathbf{6})]^{2+}$ with a 100-fold excess of t-BuOOH and rapid freezing. The low-field EPR features obtained with $g = 7.5$, 5.7, and 4.3 are reminiscent of those obtained with $[Fe(\mathbf{3})]^{2+}$ and $[Fe(\mathbf{4})]^{2+}$ consistent with a seven-coordinate high spin iron(III) center in intermediate symmetry assignable to $[Fe(\mathbf{6})(OOBu\text{-}t)]^{2+}$ [2, 27] along with a sharp signal at $g = 2.02$ for the t-butylperoxyl radical. Appearance of the low-field EPR features correlated directly with the presence of the intense blue color. However, what is remarkable here is that after standing for 2 h at 25°C, both sets of features are still present in the EPR spectrum as obtained from the solution upon re-freezing (figure 12b). Since the t-butylperoxyl radical has a half-life of only a few seconds at 25°C its persistence in the solution must be as a direct result of its continuing generation as a result of slow decay of the peroxo complex $[Fe(\mathbf{6})(OOBu\text{-}t)]^{2+}$.

3.2.3. Catalysis of cyclohexane oxygenation with H_2O_2. Table 1 summarizes the results of oxygenation by H_2O_2 on cyclohexane catalyzed by the iron(II) complexes of **3**–**7** together with data for the 6-Me-substituted TPA complexes;

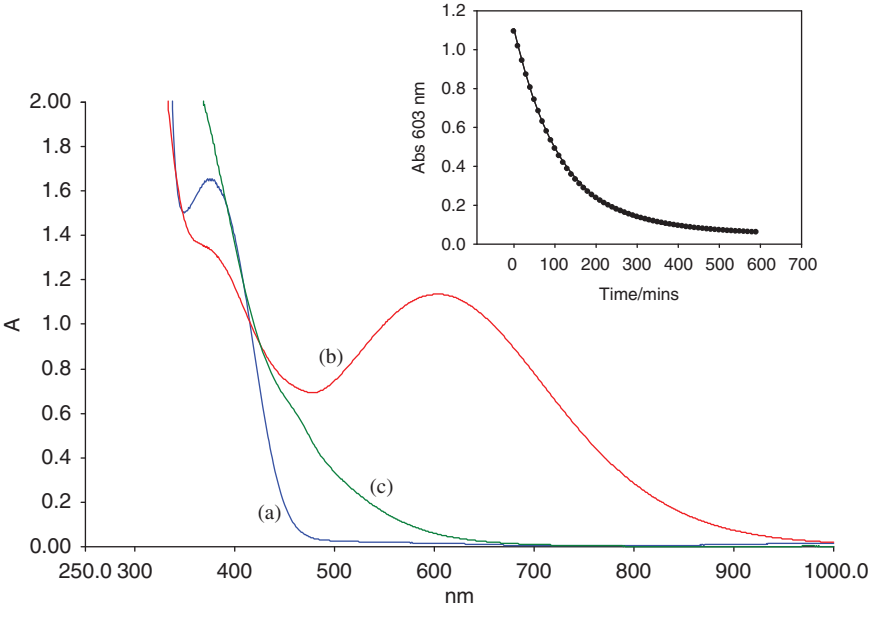

Figure 11. UV-Vis spectra for a 1.2×10^{-3} mol dm^{-3} solution of (a) [Fe(**6**)]$^{2+}$; (b) following addition of a 100-fold excess of t-BuOOH; and (c) final spectrum after the decay of (b). (inset – exponential fit of the decay of (b) to (c) monitored at 603 nm, 25°C).

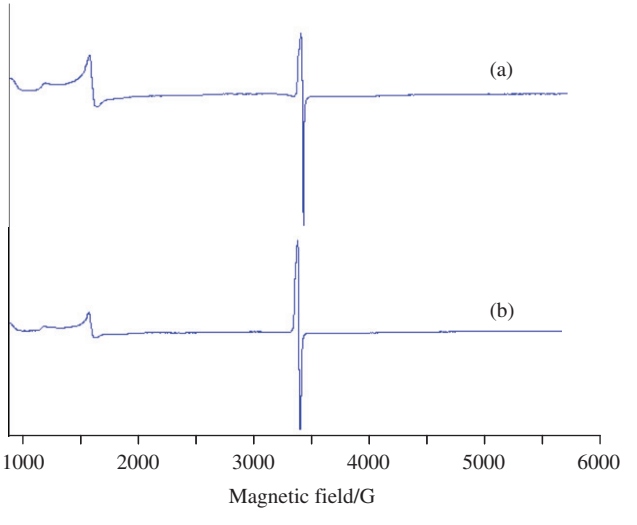

Figure 12. Frozen-glass X-band EPR spectra (110 K, CH_3CN solvent) of (a) [Fe(**6**)]$^{2+}$ (3×10^{-4} mol dm^{-3}) following the addition of 100-fold excess of t-BuOOH and (b) following warming to 25°C for 2 h.

[Fe(6-MeTPA)$(CH_3CN)_2$]$^{2+}$, [Fe(6-Me$_2$TPA)$(CH_3CN)_2$]$^{2+}$, [Fe(6-Me$_3$TPA)$(CH_3CN)_2$]$^{2+}$, and simple iron(II) salts for comparison. Under the comparable conditions, the iron(II) complexes of **3**–**7** were somewhat inferior as catalysts toward oxidation of cyclohexane by H_2O_2 in CH_3CN solution compared with unsubstituted

Table 1. Results of catalytic H_2O_2 oxygenation of cyclohexane by iron(II) complexes of **3**–**7** in CH_3CN at 25°C along with those from related iron(II) complexes and simple salts.

Iron(II) catalyst	Equivalent H_2O_2[a]	Equivalent C_6H_{10}	Efficiency[b]	TN[c]	A/K[d]	KIE[e]	3°/2°[f,g]	References
$[Fe(\mathbf{3})]^{2+}$	10	1000	6.4	0.6	1.6	–	–	This study
	100	1000	1.8	1.8	1.6	–	–	This study
$[Fe(\mathbf{4})]^{2+}$	100	1000	3.0	3.0	1.2	–	–	This study
$[Fe(\mathbf{5})(CH_3CN)]^{2+}$	10	1000	5.1	0.5	0.8	–	–	This study
	100	1000	2.3	2.3	2.1	–	–	This study
$[Fe(\mathbf{6})]^{2+}$	100	1000	1.4	1.4	3.3	–	–	This study
$[Fe(\mathbf{7})(CH_3CN)_2]^{2+}$	100	1000	4.6	4.6	3.1	–	–	This study
$[Fe(TPA)(CH_3CN)_2]^{2+}$ **1**	10	1000	37	3.7	5.0	3.5	17	[3]
$[Fe(6\text{-}MeTPA)(CH_3CN)_2]^{2+}$	10	1000	40	4.0	7.0	3.6	30	[3]
$[Fe(6\text{-}Me_2TPA)(CH_3CN)_2]^{2+}$	10	1000	29	2.9	2.0	4.0	33	[3]
$[Fe(6\text{-}Me_3TPA)(CH_3CN)_2]^{2+}$	10	1000	14	1.4	1.0	3.3	15	[3]
$[Fe(N4py)(CH_3CN)]^{2+}$	10	1000	31	3.1	1.4	1.5	3.3	[31]
	100	1000	9.6	9.6	1.3	–	–	[31]
$[Fe(CH_3CN)_4]^{2+}$	10	1000	10	1.0	1.0	1.8	–	[34]
$Fe(ClO_4)_3$	10	1000	37	3.7	1.9	1.5	3.3	[28]
$OH^{\bullet}$ radical			1.0		1–2	2	2.0	[28, 30]

[a]H_2O_2 added by syringe pump in the air at 25°C over 30 min, total incubation time 35 min before work up, [b]efficiency 100 × (cyclohexanol + cyclohexanone)/H_2O_2, [c]TN, mols oxidized products/mols catalyzed, [d]A/K, cyclohexanol/cyclohexanone, [e]KIE, kinetic isotope effect of cyclohexanol formation (C_6H_{12} *vs.* C_6D_{12}), [f]3°/2°, 1-adamantanol/(2-adamantanol + 2-adamantanone) corrected for the number of C–H bonds, and [g]Fe/H_2O_2/alkane = 1/10/10 (adamantane).

TPA in **1** [3]. The iron(II) complexes of **3**, **4**, and **6** generate high spin peroxoiron(III) intermediates. Such species would be expected to facilitate O-radical-based processes *via* homolytic Fe–O cleavage [1, 21]. For $[Fe(\mathbf{3})]^{2+}$ and $[Fe(\mathbf{4})]^{2+}$, this is reflected in low A/K ratios (1.2 : 1.6) comparable to those obtained from oxidation by free HO radicals [28, 30]. $[Fe(\mathbf{5})(CH_3CN)]^{2+}$, with only one 6-py substituent, however, generates low spin peroxoiron(III) intermediates (EPR, 110 K) with both H_2O_2 and t-BuOOH, prior to the eventual formation of a stable high spin iron(III) product. Therefore, some degree of comparable activity to **1** was expected. However, the similarly poor activity and selectivity (maximum A/K 2.1) indicates again largely O-radical-derived products reminiscent of the behavior seen for pentadentate $[Fe(N4py)(CH_3CN)]^{2+}$ which shows similarly poor activity despite generating low spin peroxoiron(III) intermediates [31]. Here, subsequent characterization of the oxo–iron(IV) complex $[Fe(O)(N4py)]^{2+}$ [32] suggests formation of the O radicals *via* homolytic O–O rather than Fe–O cleavage. In separate studies, $[Fe(O)(N4py)]^{2+}$ has been shown to be a rather sluggish oxidant toward the hydroxylation of alkane C–H bonds [32], a feature attributable to its coordination saturation. Indeed, $[Fe(O)(N4py)]^{2+}$ is one of the longest lived oxo–iron(IV) complexes known with a reported half-life of ~60 h at 25°C [32(b)]. As a result, the products of reaction with HO. (RO.) radicals dominate. Given the evidence for urea carbonyl coordination in $[Fe(\mathbf{6})]^{2+}$ (NMR, confirmed by X-ray), it is likely that similar coordination occurs in $[Fe(\mathbf{5})(CH_3CN)]^{2+}$ (as suggested by NMR, see figures S7 and S8) resulting in coordination saturation for any putative $[Fe(O)(\mathbf{5})]^{2+}$ species formed (1, 2) akin to $[Fe(O)(N4py)]^{2+}$. In the case of $[Fe(\mathbf{5})(CH_3CN)]^{2+}$, we have been unable to confirm this by X-ray crystallography.

Finally, complexes $[Fe(\mathbf{6})]^{2+}$ and $[Fe(\mathbf{7})(CH_3CN)_2]^{2+}$ [33] are worthy of further mention. Both give rise to the highest level of selectivity to cyclohexanol (A/K ratio > 3) seen to date for a *bis*(6-py)- or *tris*(6-py)-substituted iron–TPA complex which

tentatively suggests involvement of a high-valent oxo–iron reactant. For $[Fe(\mathbf{6})]^{2+}$, the likelihood that the two coordinated urea carbonyls (X-ray evidence here) are retained upon oxidation to iron(III) (harder) suggests that short-lived high spin $[Fe(\mathbf{6})(OOH)]^{2+}$ (not observed) might be seven-coordinate, as deduced below for $[Fe(\mathbf{6})(OOBu\text{-}t)]^{2+}$, wherein O–O cleavage to yield a high-valent oxo–iron species might be facilitated by protonation of the departing OH group *via* hydrogen-bonding to the proximal urea N–H (figure 13). The longer life time of $[Fe(\mathbf{5})(OOH)]^{2+}$ compared with $[Fe(\mathbf{6})(OOH)]^{2+}$ is believed due to the low spin six-coordinate nature of the former and the presence of only one potential hydrogen-bonding ureido group.

A low symmetry seven-coordinate structure is also implied for the longer lived peroxo complex, $[Fe(\mathbf{6})(OOBu\text{-}t)]^{2+}$, from the similarity of its EPR spectrum to that of the crystallographically characterized seven-coordinate *bis*-(6-pivalylamido)–TPA complex, $[Fe(BPPA)(O_2CMe_3)]^{2+}$ (figure 14a) (low-field features at $g = 7.6$, 5.8, and 4.3), and the long-lived peroxo complex $[Fe(BPPA)(OOBu\text{-}t)]^{2+}$ (figure 14b) [26]. The marked

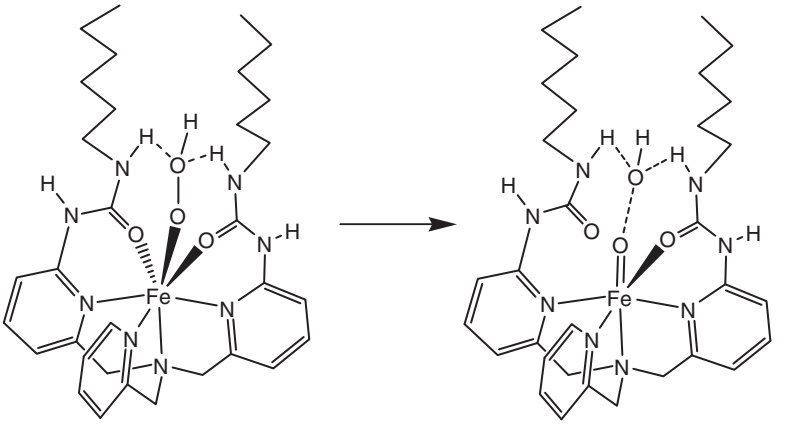

Figure 13. Possible facilitation of oxo-iron formation from $[Fe(\mathbf{6})(OOH)]^{2+}$ *via* urea N–H hydrogen bonded assisted departure of "OH".

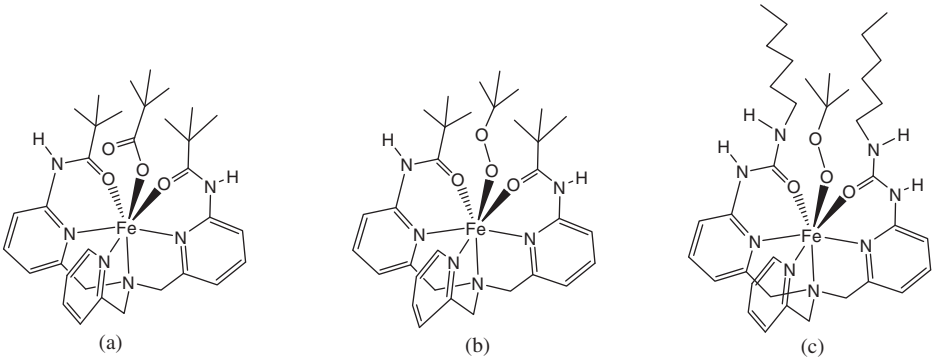

(a) $[Fe(BPPA)(O_2CCMe_3)]^{2+}$

(b) $[Fe(BPPA)(OOBu\text{-}t)]^{2+}$

(c) $[Fe(\mathbf{6})(OOBu\text{-}t)]^{2+}$

Figure 14. Structures of seven-coordinate high spin iron(III) complexes of BPPA [25] and **6**.

stability of the t-butylperoxoiron(III) complexes of BPPA and **6** is intriguing and may be related to a degree of steric protection provided for the OOBu-*t* group toward O–O or Fe–O cleavage coupled with a lack of H-bonded assistance to cleavage.

Despite the highest A/K ratio yet seen for cyclohexane oxidation by H_2O_2 catalyzed by a *bis*-6-py-substituted iron(II)–TPA complex in the case of $[Fe(\mathbf{6})]^{2+}$, the overall catalytic activity is still somewhat inferior to that shown by **1**. We believe this is attributable to the formation of high spin peroxo complexes and the presence of coordination saturation (absence of the two essential labile *cis* coordination sites [14]). The similarly poor activity shown by high spin $[Fe(\mathbf{3})]^{2+}$ and $[Fe(\mathbf{4})]^{2+}$ is likewise believed to be directly related to EPR evidence for high spin seven-coordination (retention of ether oxygen coordination) in $[Fe(\mathbf{3})(OOBu\text{-}t)]^{2+}$ and $[Fe(\mathbf{4})(OOBu\text{-}t)]^{2+}$.

Finally, somewhat unexpectedly, the *tris*(6-bromo)–TPA derivative $[Fe(\mathbf{7})(CH_3CN)_2]^{2+}$ shows the highest activity of all the iron(II) 6-py-substituted TPA complexes studied in terms of turnover and efficiency of incorporation of oxygen from H_2O_2 into products. The behavior here, if marginal, is surprising given the electron-withdrawing nature and steric bulk of the 6-bromo substituents. Here, the spin state of the intermediate peroxo species has not been investigated separately, although given the steric bulk of the 6-bromo substituents, the formation of high spin peroxoiron(III) species would be anticipated.

Que and co-workers have previously shown that introduction of two or more 6-substituents on the py groups of TPA induces a change in spin state of the iron(II) complex from low spin for $[Fe(TPA)(CH_3CN)_2]^{2+}$ and $[Fe(6\text{-}MeTPA)(CH_3CN)_2]^{2+}$ to high spin for $[Fe(6\text{-}Me_2TPA)(CH_3CN)_2]^{2+}$, and $[Fe(6\text{-}Me_3\text{-}TPA)(CH_3CN)_2]^{2+}$ [23] with correspondingly poorer catalytic activity toward cyclohexane oxygenation by H_2O_2 [3]. As observed here, those complexes generating high spin peroxoiron(III) intermediates lead to low A/K ratios (from cyclohexane) suggestive of O-radical involvement, whereas those generating low spin peroxoiron(III) intermediates show evidence, in the absence of coordination saturation, of metal–oxo-derived products (higher A/K (cyclohexane) and $3^o/2^o$ (adamantane) ratios little influenced by O_2).

4. Conclusion

Introduction of substituents at the 6-position on two or more of the TPA pyridine rings in the iron(II) complexes of **3**, **4**, and **6** leads to generally poor catalytic activity (low TN and A/K ratio) compared to **1** toward catalysis of oxygenation on cyclohexane by H_2O_2. This is attributable to formation of high spin $[Fe((6\text{-}R\text{-}py)_nTPA)(OOR)]^{2+}$ species which promote Fe–O cleavage processes leading to O-radical-derived products. For monosubstituted $[Fe(\mathbf{5})(CH_3CN)]^{2+}$, a low spin peroxo complex, $[Fe(\mathbf{5})(OOR)]^{2+}$, is observed wherein the poor catalytic activity here is attributable (NMR, ES–MS evidence) to the presence of pentadentate coordination of **5** in $[Fe(\mathbf{5})(CH_3CN)]^{2+}$ and in $[Fe(\mathbf{5})(OOR)]^{2+}$ (EPR). Here, the absence of the additional labile *cis* coordination site leads to promotion of homolytic rather than heterolytic O–O cleavage generating $RO^{\bullet}$ alongside $[Fe(O)(\mathbf{5})]^{2+}$. The poor oxygenating ability of $[Fe(O)(\mathbf{5})]^{2+}$ is attributed, as for $[Fe(O)(N4py)]^{2+}$, to its coordination saturation leading to oxygenation products derived mostly from $RO^{\bullet}$ (low TN and A/K ratio). It appears that the effect of introducing the *n*-hexylureido substituents at the 6-position of the py rings of TPA

(ligands **5** and **6**) to facilitate hydrogen-bond-assisted heterolytic O–O cleavage within $[Fe(L)(OOH)]^{2+}$ intermediates has been overridden by saturation of the coordination sphere as a result of urea carbonyl coordination along with a steric weakening of the TPA ligand field resulting in generation of high spin $[Fe(L)(OOH)]^{2+}$ species. Evidence for pendent ether oxygen coordination along with a similar steric weakening of the ligand field in the iron(II)/(III) complexes of **3** and **4** similarly reduces their effectiveness as catalysts for H_2O_2 activation.

Acknowledgments

G. Guisado-Barrios thanks EPSRC for the award of a project studentship. We also thank Professors J.C. Walton (St. Andrews) and G.J.P. Britovsek (Imperial College, London) for help with the X-band EPR and oxygenation catalysis experiments, respectively.

References

[1] M. Costas, M.P. Mehn, M.P. Jensen, L. Que Jr. *Chem. Rev.*, **104**, 949 (2004).
[2] (a) K. Chen, M. Costas, J. Kim, A.K. Tipton, L. Que, Jr. *J. Am. Chem. Soc.*, **124**, 3026 (2002); (b) M. Costas, A.K. Tipton, K. Chen, D.-H. Jo, L. Que, Jr. *J. Am. Chem. Soc.*, **123**, 6722 (2001).
[3] (a) K. Chen, M. Costas, L. Que, Jr. *Dalton Trans.*, 672 (2002); (b) K. Chen, L. Que, Jr. *J. Am. Chem. Soc.*, **123**, 6327 (2001).
[4] C. Kim, K. Chen, J. Kim, L. Que Jr. *J. Am. Chem. Soc.*, **119**, 5964 (1997).
[5] K. Chen, L. Que Jr. *Chem. Commun.*, 1375 (1999).
[6] J. Kim, R.G. Harrison, C. Kim, L. Que Jr. *J. Am. Chem. Soc.*, **118**, 4373 (1996).
[7] M.H. Lim, J.-U. Rohde, A. Stubna, M.R. Bukowski, M. Costas, R.Y.N. Ho, E. Munck, W. Nam, L. Que Jr. *Proc. Natl. Acad. Sci. USA*, **100**, 3665 (2003).
[8] G.J.P. Britovsek, J. England, A.J.P. White. *Inorg. Chem.*, **44**, 8125 (2005).
[9] (a) I.V. Korendovych, S.V. Kryatov, E.V. Rybak-Akimova. *Acc. Chem. Res.*, **40**, 510 (2007); (b) S. Taktak, M. Flook, B.M. Foxman, L. Que Jr, E.V. Rybak-Akimova. *Chem. Commun.*, 5301 (2005).
[10] (a) P. Comba, G. Rajaraman. *Inorg. Chem.*, **47**, 78 (2008); (b) J. Bautz, P. Comba, C. Lopez de Laorden, M. Menzel, G. Rajaraman. *Angew. Chem. Int. Ed.*, **46**, 8067 (2007); (c) P. Comba, G. Rajaraman, H. Rohwer. *Inorg. Chem.*, **46**, 3826 (2007).
[11] (a) O.Y. Lyakin, K.P. Bryliakov, G.J.P. Britovsek, E.P. Talsi. *J. Am. Chem. Soc.*, **131**, 10798 (2009); (b) E.A. Duban, K.P. Brylyakov, E.P. Talsi. *Kinet. Catal.*, **49**, 379 (2008); (c) E.A. Duban, K.P. Bryloakov, E.P. Talsi. *Eur. J. Inorg. Chem.*, 852 (2007).
[12] (a) JPJP Pat., 99-1287622000319291 (2000); (b) WOWO Pat., 97-US107649748710 (1997); (c) WOWO Pat., 95-EP19309534628 (1995).
[13] (a) M.P. Jensen, A. Mairata i Payeras, A.T. Fidler, M. Costas, J. Kaizer, A. Stubna, E. Munck, L. Que, Jr. *Inorg. Chem.*, **36**, 2398 (2007); (b) M.J. Park, J. Lee, Y. Suh, J. Kim, W. Nam. *J. Am. Chem. Soc.*, **128**, 2630 (2006); (c) M.P. Jensen, M. Costas, R.Y.N. Ho, J. Kaizer, A. Mariata i Payeras, E. Munck, L. Que, Jr, J.-U. Rohde, A. Stubna. *J. Am. Chem. Soc.*, **127**, 10512 (2005); (d) J. Paine, M. Costas, J. Kaizer, L. Que, Jr. *J. Biol. Chem.*, **11**, 272 (2006); (e) J. Kaizer, M. Costas, L. Que, Jr. *Angew. Chem. Int. Ed.*, **42**, 3671 (2003).
[14] (a) R. Mas-Balleste, L. Que, Jr. *J. Am. Chem. Soc.*, **129**, 15964 (2007); (b) X. Shen, L. Que, Jr. *Chem. Commun.*, 2209 (2008).
[15] Y. Feng, C.-Y. Ke, G. Xue, L. Que Jr. *Chem. Commun.*, 50 (2009).
[16] N. Raffard, V. Balland, J. Simaan, S. Létard, M. Nierlich, K. Miki, F. Banse, E. Anxolabéhère-Mallart, J.-J. Girerd. *C. R. Chimie*, **5**, 99 (2002).
[17] (a) J.M. Thomas, R. Raja, G. Sankar, R.G. Bell. *Acc. Chem. Res.*, **34**, 191 (2001); (b) R.S. Drago. *Coord. Chem. Rev.*, **117**, 185 (1992).
[18] M.B. Fisher, Y.-M. Zheng, A.E. Rettie. *Biochem. Biophys. Res. Commun.*, **248**, 352 (1998).
[19] R.G. Mathys, A. Schmid, B. Witholt. *Biotechnol. Bioeng.*, **64**, 459 (1999).

[20] M.W. Peters, P. Meinhold, A. Glieder, F.H. Arnold. *J. Am. Chem. Soc*., **125**, 13442 (2003).
[21] M. Costas, K. Chen, L. Que Jr. *Coord. Chem. Rev*., **200–202**, 517 (2000).
[22] K.S. Hagen. *Inorg. Chem*., **39**, 5867 (2000).
[23] Y. Zang, J. Kim, Y. Dong, E.C. Wilkinson, E.H. Appelman, L. Que Jr. *J. Am. Chem. Soc*., **119**, 4197 (1997).
[24] D.G. Lonnon, G.E. Ball, I. Taylor, D.C. Craig, S.B. Colbran. *Inorg. Chem*., **48**, 4863 (2009).
[25] R.H. Fish, M.S. Konings, K.J. Oberhausen, R.H. Fong, W.M. Yu, G. Christou, J.B. Vincent, D.K. Coggin, R.M. Buchanan. *Inorg. Chem*., **30**, 3002 (1991).
[26] A. Wada, S. Ogo, Y. Watanabe, M. Mukai, T. Kitagawa, K. Jitsukawa, H. Masuda, H. Einaga. *Inorg. Chem*., **38**, 3592 (1999).
[27] G. Guisado-Barrios, Y. Li, A.M.Z. Slawin, D.T. Richens, I.A. Gass, P.R. Murray, L.J. Yellowlees, E.K. Brechin. *Dalton Trans*., 551 (2008).
[28] A.F. Trotman-Dickenson. *Adv. Free-Radical Chem*., **1**, 1 (1965).
[29] D.T. Richens, S.L. Jain, A.C. Gale. *Inorg. React. Mech*., **6**, 169 (2007).
[30] (a) C. Walling. *Acc. Chem. Res*., **8**, 125 (1975); (b) G.V. Buxton, C.L. Greenstock, W.P. Helman, A.B. Ross. *J. Phys. Chem. Ref. Data*, **17**, 513 (1988); (c) S. Miyajima, O. Simamura. *Bull. Chem. Soc. Jpn*., **48**, 533 (1975).
[31] T.A. van den Berg, J.W. de Boer, W.R. Browne, G. Roelfes, B.L. Feringa. *Chem. Commun*., 2550 (2004).
[32] (a) K. Ray, S.M. Lee, L. Que, Jr. *Inorg. Chim. Acta*, **261**, 1066 (2008); (b) J. Kaizer, E.J. Klinker, N.Y. Oh, J.-U. Rohde, W.J. Song, A. Stubna, J. Kim, E. Munck, W. Nam, L. Que, Jr. *J. Am. Chem. Soc*., **126**, 472 (2004).
[33] The formula $[Fe(\mathbf{7})(CH_3CN)_2]^{2+}$ was assumed on the basis of comparisons with the structurally characterized high spin complex $[Fe(6\text{-}Me_3TPA)(CH_3CN)_2]^{2+}$.
[34] H.C. Tung, C. Kang, D.T. Sawyer. *J. Am. Chem. Soc*., **114**, 3445 (1992).